ARTICLES SCIENCE CHINA Materials

mater.scichina.com link.springer.com

Published online 18 August 2016 | doi: 10.1007/s40843-016-5097-7
*Sci China Mater* 2016, 59(8): 618–628

# Enhanced electrochemical performance of Li-rich low-Co $Li_{1.2}Mn_{0.56}Ni_{0.16}Co_{0.08-x}Al_xO_2$ ($0 \le x \le 0.08$) as cathode materials

Ting-Feng Yi*, Xiao Han, Shuang-Yuan Yang and Yan-Rong Zhu

**ABSTRACT** **Layered $Li_{1.2}Mn_{0.56}Ni_{0.16}Co_{0.08-x}Al_xO_2$ ($0 \le x \le 0.08$) cathode materials were successfully synthesized by a sol-gel method. X-ray diffraction and the refinement data indicate that all materials have typical α-$NaFeO_2$ structure with *R*-3*m* space group, and the *a*-axis has almost no change, but there is a slight decrease in the *c* lattice parameter as well as the cell volume. Scanning electron microscopy and high resolution transmission electron microscopy prove that all the samples have uniform particle size of about 200–300 nm and smooth surface. The energy-dispersive X-ray spectroscopy mapping shows that aluminum has been homogeneously doped in the $Li_{1.2}Mn_{0.56}Ni_{0.16}Co_{0.08}O_2$ cathode material. The cyclic voltammetry and electrochemical impedance spectroscopy reveal that appropriate Al-doping contributes to the reversible lithium-ion insertion and extraction, and then reduces the electrochemical polarization and charge transfer resistance. $Li_{1.2}Mn_{0.56}Ni_{0.16}Co_{0.08-x}Al_xO_2$ ($x$ = 0.05) shows the lowest charge transfer resistance and the highest lithium-ion diffusion coefficient among all the samples. The Li-rich electrodes with low-level Al doping shows a much higher discharge capacity than the pristine one, especially the $Li_{1.2}Mn_{0.56}Ni_{0.16}Co_{0.08-x}Al_xO_2$ ($x$ = 0.05) sample, which exhibits greater rate capacity and better fast charge-discharge performance than the other samples. $Li_{1.2}Mn_{0.56}Ni_{0.16}Co_{0.08-x}Al_xO_2$ ($x$ = 0.05) also exhibits higher discharge capacity than the pristine one at each cycle at 55°C. These results clearly indicate that the high rate capacity together with a good high rate cycling performance and high-temperature performance of the low-Co $Li_{1.2}Mn_{0.56}Ni_{0.16}Co_{0.08-x}Al_xO_2$ ($x$=0.05) is a promising alternative to next-generation lithium-ion batteries.**

**Keywords:** Lithium-ion battery, $Li_{1.2}Mn_{0.56}Ni_{0.16}Co_{0.08-x}Al_xO_2$, cycling stability, fast charge-discharge performance, high-temperature performance

## INTRODUCTION

Lithium-ion batteries (LIBs) have been considered as one of the most promising energy storage devices due to their high energy density, light weight and high operating voltage and long cycle life [1–4]. However, as a power source for electric vehicles (EVs), hybrid electric vehicles (HEVs) and plug-in hybrid electric vehicles (PHEVs), it is of great essentiality to develop satisfactory cathode materials with high energy density and cycling stability [5–7]. The energy density of a cathode is closely related to the capacity and operating voltage. Recently, Li-rich layered oxides with a chemical formula of $xLi_2MnO_3{\cdot}(1-x)LiMO_2$ (M = Co, Mn, Ni) have drawn much attention as attractive alternatives because they possess superior capacity over 250 mA h $g^{-1}$ and higher power density compared with traditional cathode materials $LiFePO_4$, $LiMn_2O_4$ and $LiCoO_2$ [8,9]. Unfortunately, Li-rich materials still suffer from low initial Coulombic efficiency, poor cycle performance and low rate capability, which hinder the progress of their popularization in practical application [10]. Recently, many investigators have made great efforts including surface modification [11,12], cation and anion doping [13–16] or fabrication of nano-sized particles [17–19] to improve the electrochemical performance of the layered Li-rich cathode materials. As we know, the nanostructured material often reduces the volumetric energy density of the full batteries because of the large specific surface area. Moreover, a uniform surface coating around the whole active particles is also obviously difficult to achieve. Hence, doping has been considered an effective way to improve the electrochemical performance of electrode materials. Many researchers have reported that electrochemical performance of $xLi_2MnO_3{\cdot}(1-x)LiMO_2$ is closely related to the $x$ value. Finding a new and promising Li-rich cathode material composition is a main research topic because

School of Chemistry and Chemical Engineering, Anhui University of Technology, Maanshan 243002, China
* Corresponding author (email: tfyihit@163.com)

of the overall effect on the electrochemical performance of batteries [20–23]. Taking into account the cost, low Co-based Li-rich material with high content of Mn should be developed. However, the Co-free Li-rich material usually suffers from poorer rate capability [24] because the presence of cobalt in materials can greatly enhance the oxygen loss, reduce the replacement of lithium and nickel, and effectively promote $Li_2MnO_3$ activation [25–27]. Developing doped high-performance Li-rich material using earth-abundant elements is more desirable and noble metals (such as Ru, Ag, etc.)-free cathodes are some of the most attractive choices used in commercial LIBs [28]. It is well known that Al is abundant and less expensive than many other transition metals, so the Al doped Li-rich material with the substitution of $Co^{3+}$ by $Al^{3+}$ is expected to be a cathode material with lower cost than other high Co-based Li-rich material. Meanwhile, the bond energy of the Al–O (512 kJ $mol^{-1}$) is much greater than that of Mn–O (402 kJ $mol^{-1}$), so it has a higher octahedral site preference energies (OPE) which results in diminution of the bond length [29] and thus benefits the structural stability. It has been reported that the electrode material prepared by sol-gel method has some common features: fine particle size, narrow size distribution, and uniform composition, which usually make high electrochemical performance [30–32].

In this work, aluminum substituted low Co-based Li-rich materials ($Li_{1.2}Mn_{0.56}Ni_{0.16}Co_{0.08-x}Al_xO_2$ ($0 \le x \le 0.08$)) were synthesized by a sol-gel method, and their electrochemical performance was studied. The Al doping may further lower the content of Co which is relatively expensive and toxic. This will not only lower the production cost, but it will also be more environmentally friendly.

## EXPERIMENTAL

### Material synthesis

The layered ($Li_{1.2}Mn_{0.56}Ni_{0.16}Co_{0.08-x}Al_xO_2$ ($x$=0, 0.01, 0.02, 0.05 and 0.08) materials were synthesized by a sol-gel method, and the preparation process is given in Scheme 1. Stoichiometric amounts of $Co(CH_3COO)_2{\cdot}4H_2O$ (99.5%, Aladdin Chemistry Co., Ltd.), $Mn(CH_3COO)_2{\cdot}4H_2O$ (99%, Aladdin Chemistry Co., Ltd.), $Ni(CH_3COO)_2{\cdot}4H_2O$ (99%, Aladdin Chemistry Co., Ltd.), $Al(NO_3)_3{\cdot}4H_2O$ (99%, Aladdin Chemistry Co., Ltd.), and an excess amount $LiCH_3COO{\cdot}H_2O$ (5% in molar ratio, 99.5%, Aladdin Chemistry Co., Ltd.) were dissolved in deionized water. The appropriate sugar solution was added into the mixed acetate solution with a vigorous stirring. The mixed solution was evaporated at 80°C for 8–12 h with continuous stirring to remove excess water until a gel was obtained. Then, the gel was dried in vacuum drying oven at 120°C for 12 h, resulting in the formation of amorphous powders. The resulting powder was at first calcined at 450°C for 4 h and then calcined at 850°C for 8 h in air to obtain the final product.

### Battery preparation

A CR2025 coin-cell assembly was used for the electrochemical characterization. A slurry was formed by mixing $Li_{1.2}Mn_{0.56}Ni_{0.16}Co_{0.08-x}Al_xO_2$ ($0 \le x \le 0.08$) powders (80%), super P conductive carbon (10%), and the binder (10 wt.% polyvinylidene fluoride, dissolved in *N*-methyl-2-pyrrolidone). After being coated onto the Al foil, the film was dried in a vacuum oven at 110°C for 12 h and then cut into discs with a radius of 7 mm. The thickness of the prepared electrode in this work is about 30 μm. The half-cells were assembled with active material and a metallic Li anode separated by porous polypropylene film (Celgard 2300) filled with 1 mol $L^{-1}$ $LiPF_6$ in ethylene carbonate/dimethyl carbonate (1:1 *v*/*v*) solution.

### Material characterization and electrochemical measurements

The crystal structure of all powders was characterized by

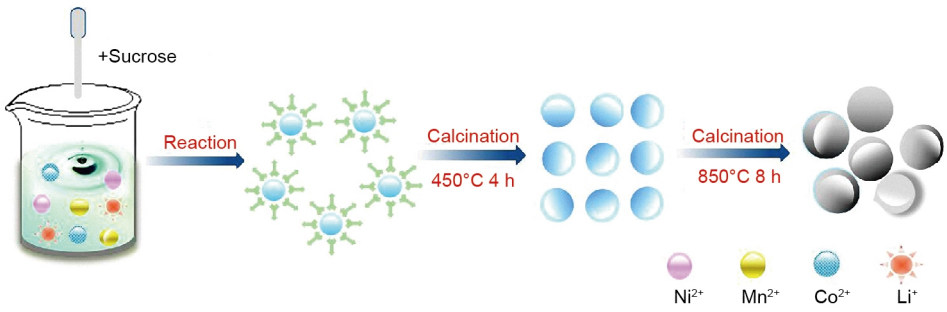


**Scheme 1** Schematic of the preparation process of $Li_{1.2}Mn_{0.56}Ni_{0.16}Co_{0.08}O_2$.

X-ray powder diffraction (XRD) on a Rigaku instrument with Cu Kα radiation. The particle morphology was observed using a scanning electron microscope (SEM, SU8000) and a high resolution transmission electron microscope (HRTEM) (JEOL JEM-2010). The cyclic voltammetry (CV) test was carried out on a CHI 1000C electrochemical workstation with a voltage between 2.0 and 4.8 V at a scanning rate of 0.2 mV $s^{-1}$. Electrochemical impedance spectroscopy (EIS) tests were performed on a Princeton P4000 electrochemical working station in the frequency range of 100 kHz to 10 mHz. The galvanostatic charge-discharge tests were performed on LAND CT2001A (Wuhan Jinnuo) between 2.0 and 4.8 V (*vs.* $Li^+/Li$) at different rates and temperatures.

## RESULTS AND DISCUSSION

Fig. 1 shows the XRD patterns of the synthesized $Li_{1.2}Mn_{0.56}Ni_{0.16}Co_{0.08-x}Al_xO_2$ ($0 \le x \le 0.08$) powders. The sharp and well-defined peaks indicate that all materials have pure layer structure, which can be indexed to the hexagonal α-$NaFeO_2$ structure with *R*-3*m* space group. $Al_2O_3$ impurity peaks are not observed in all samples, indicating that Al doping does not change the crystal structure of Li-rich material. The high-purity characteristics of the as-prepared samples can also be confirmed by the XRD Rietveld refinement results as displayed in Fig. 2. Several extra small peaks between 20° and 25° are also observed, which originate from the superlattice ordering of Li and Mn in the transition metal (TM) layers, and these results prove the existence of $Li_2MnO_3$(*C*2/*m*) [33]. It has been reported that the integral intensity ratio between (003) and (104) peaks can reflect cation mixing [34]. When the ratio of $I_{(003)}/I_{(104)}$ is less than 1.2, there is an undesirable level of cation mixing [35]. The values of $I_{(003)}/I_{(104)}$ are 0.795, 0.901, 0.955, 1.239 and 1.813, respectively. Obviously, the cation mixing of the Li-rich material decreases because of Al doping. The refinement data indicate that the *a*-axis has almost no change, but there is a slight decrease in the *c* lattice parameter as well as the cell volume. This is attributed to the smaller ionic radius of $Al^{3+}$ (0.0535 nm) compared with the ionic radius of $Co^{3+}$ (0.061 nm) [36].

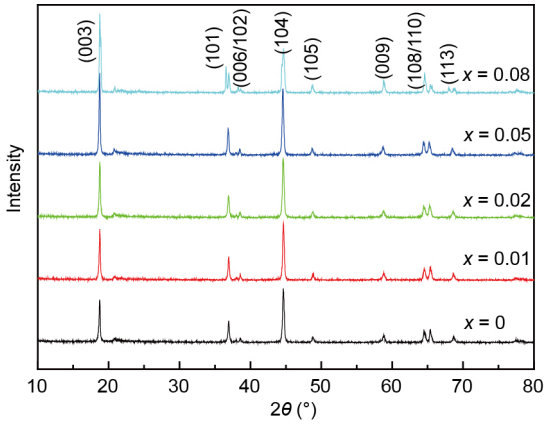


**Figure 1** XRD patterns of $Li_{1.2}Mn_{0.56}Ni_{0.16}Co_{0.08-x}Al_xO_2$ ($0 \le x \le 0.08$).

Figs 3a–e show the scanning electron microscopy (SEM) images of $Li_{1.2}Mn_{0.56}Ni_{0.16}Co_{0.08-x}Al_xO_2$ ($0 \le x \le 0.08$) powders. It can be found that the morphologies of all samples are similar, and all samples show uniform particle distribution. The size of all materials is about 200–300 nm, and the Al doping does not affect the morphology of Li-rich material. These results indicate sufficient contact between the active materials and the electrolyte which is favorable for lithium ions transfer coefficient in the cathode. The detailed microstructure of $Li_{1.2}Mn_{0.56}Ni_{0.16}Co_{0.08-x}Al_xO_2$ ($x$=0.05) is shown in the TEM images in Figs 3f–h. It can be found that the size of a $Li_{1.2}Mn_{0.56}Ni_{0.16}Co_{0.08-x}Al_xO_2$ ($x$=0.05) material is about 200 nm, and a lattice fringe of approximately 0.466 nm can be observed, which corresponds to the (003) and/or (001) interlayer spacing for rhombohedral $LiMO_2$ (M = transition metals) and/or monoclinic $Li_2MnO_3$ respectively [37,38], in good agreement with the XRD result shown in Fig. 1. The HRTEM image of Fig. 3g also shows the lattice-fringes of 0.241 nm corresponding to the inter-plane distances (−131) of the monoclinic structure component $Li_2MnO_3$ [39] or the (101) plane of the hexagonal layered structure [5]. In addition, to prove the homogeneous Al doping in the Li-rich materials, energy dispersive X-ray spectroscopy (EDS) mapping of $Li_{1.2}Mn_{0.56}Ni_{0.16}Co_{0.08-x}Al_xO_2$ ($x$=0.05) material is shown in Fig. 4. The presence of manganese, nickel, cobalt, aluminum and oxygen can be found. It can be seen that not only transition metal elements including manganese, nickel and cobalt are homogeneously distributed on the surface of the particle but also aluminum atoms are uniformly distributed in the Al-doped Li-rich material. It is therefore reasonable to infer that aluminum has been doped in the $Li_{1.2}Mn_{0.56}Ni_{0.16}Co_{0.08}O_2$ cathode material successfully and homogeneously.

Fig. 5 displays the CV and EIS tests of all cathode materials. The CV curves of the first three cycles are shown in Figs 5a–e. The initial anodic peaks of all the cathodes around 3.7–4.4 V are due to the oxidation process of $Ni^{2+}$ and $Co^{3+}$ ions to higher oxidation states. The second anodic peaks located in the potential range between 4.5 and 4.8 V are normally associated with the irreversible loss of oxygen from $Li_2MnO_3$-type component which disappears in

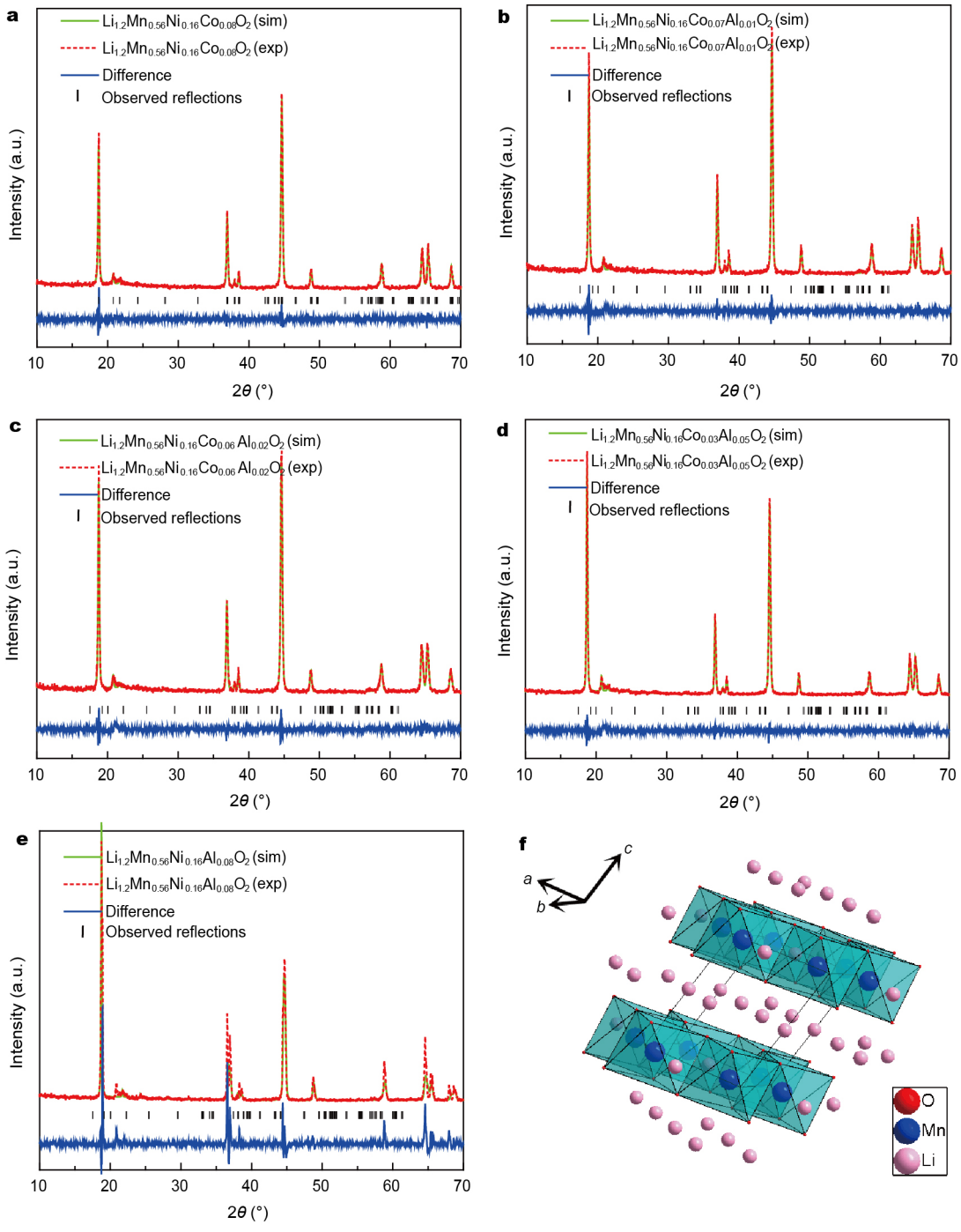


**Figure 2** XRD refinement profiles of $Li_{1.2}Mn_{0.56}Ni_{0.16}Co_{0.08-x}Al_xO_2$ (a) $x$=0, (b) $x$=0.01, (c) $x$=0.02, (d) $x$=0.05, (e) $x$=0.08 and (f) refinement model.

subsequent cycles [40]. Based on the first three cycles of CV curves, a stable current can be reached at the second cycle, as the curves of the 2nd and the 3rd cycle overlapped well, indicating that all samples may have high cycling stability at low charge-discharge rate. The voltage difference ($\Delta\varphi_p$) between the anodic peak and cathodic peak can reflect the electrochemical reversibility. As shown in Table S1, $Li_{1.2}Mn_{0.56}Ni_{0.16}Co_{0.08-x}Al_xO_2$ ($x$=0.02 and 0.05) for the first cycle exhibits the smallest $\Delta\varphi_p$ value among the five samples. It is reasonable to infer that appropriate Al-doping contributes to the reversible lithium-ion insertion and extraction, and then reduces the electrochemical polariz-

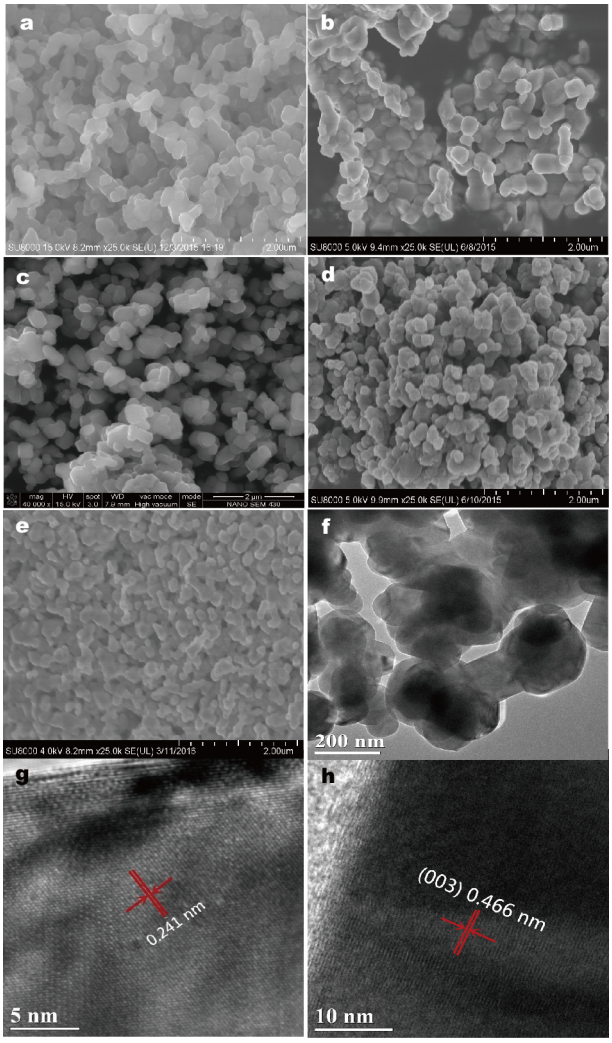


**Figure 3** SEM images of $Li_{1.2}Mn_{0.56}Ni_{0.16}Co_{0.08-x}Al_xO_2$ (a) $x$=0, (b) $x$=0.01, (c) $x$=0.02, (d) $x$=0.05, (e) $x$=0.08; and TEM images of $Li_{1.17}Mn_{0.56}Ni_{0.16}Co_{0.03}Al_{0.05}O_2$(f, g, h).

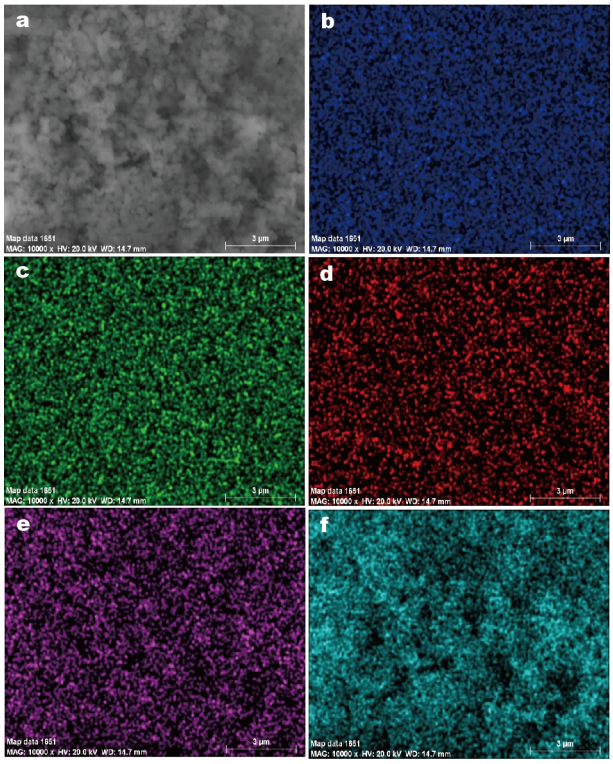


**Figure 4** EDS mapping images of $Li_2Mn_{0.56}Ni_{0.16}Co_{0.03}Al_{0.05}O_2$. (a) SEM image, (b) Mn element, (c) Ni element, (d) Co element (e) Al element and (f) O element.

ation and improves the reversibility of the cathode. This result confirms the favorable rate performance and cycling stability of the $Li_{1.2}Mn_{0.56}Ni_{0.16}Co_{0.08-x}Al_xO_2$ ($x$=0.02 and 0.05) samples. To further illuminate the effect of Al doping on the kinetics of $Li_{1.2}Mn_{0.56}Ni_{0.16}Co_{0.08}O_2$ material, EIS for all half cells before cycling were measured at $V_{OC}$ (open circuit voltage), and the corresponding Nyquist plots are given in Fig. 5f. The equivalent circuit used to fit the EIS is given in Fig. S1, and the fitting results are listed in Table S2. The intermediate-frequency semicircle always corresponds to the charge transfer resistance ($R_{ct}$), which reflects the electrochemical reaction activity at the interface and electron/ion conductivity. The low-frequency inclined line is attributed to Warburg impedance ($W$), which is related to the diffusion process of the lithium ions in the solid phase of electrode [41,42]. Obviously, $Li_{1.2}Mn_{0.56}Ni_{0.16}Co_{0.08-x}Al_xO_2$ ($0.01 \le x \le 0.05$) electrodes exhibit lower charge transfer resistance than the pristine $Li_{1.2}Mn_{0.56}Ni_{0.16}Co_{0.08}O_2$ electrode, indicating that the appropriate Al doping can decrease the charge transfer resistance of the $Li_{1.2}Mn_{0.56}Ni_{0.16}Co_{0.08}O_2$, which is favorable to the fast transport of lithium ions. It is therefore reasonable to infer that the small charge transfer resistance corresponds to the small electrochemical polarization, thus leading to excellent cycling performance. An interesting thing is that $Li_{1.2}Mn_{0.56}Ni_{0.16}Co_{0.08-x}Al_xO_2$ ($x$=0.05) shows the lowest charge transfer resistance, suggesting that it may have the highest electrochemical activity and kinetic behavior among all samples during cycling. This also matches the results of the cyclic performance shown in Figs 6c and d. However, a dramatic increase of charge transfer resistance is noted for $Li_{1.2}Mn_{0.56}Ni_{0.16}Co_{0.08-x}Al_xO_2$ ($x$=0.08) compared to the other Li-rich materials. Hence, the doping contents of Al need to be optimized. The lithium-ion diffusion coefficient ($D_{Li}$) can be calculated from the plots in the low-frequency region, which represents the diffusion

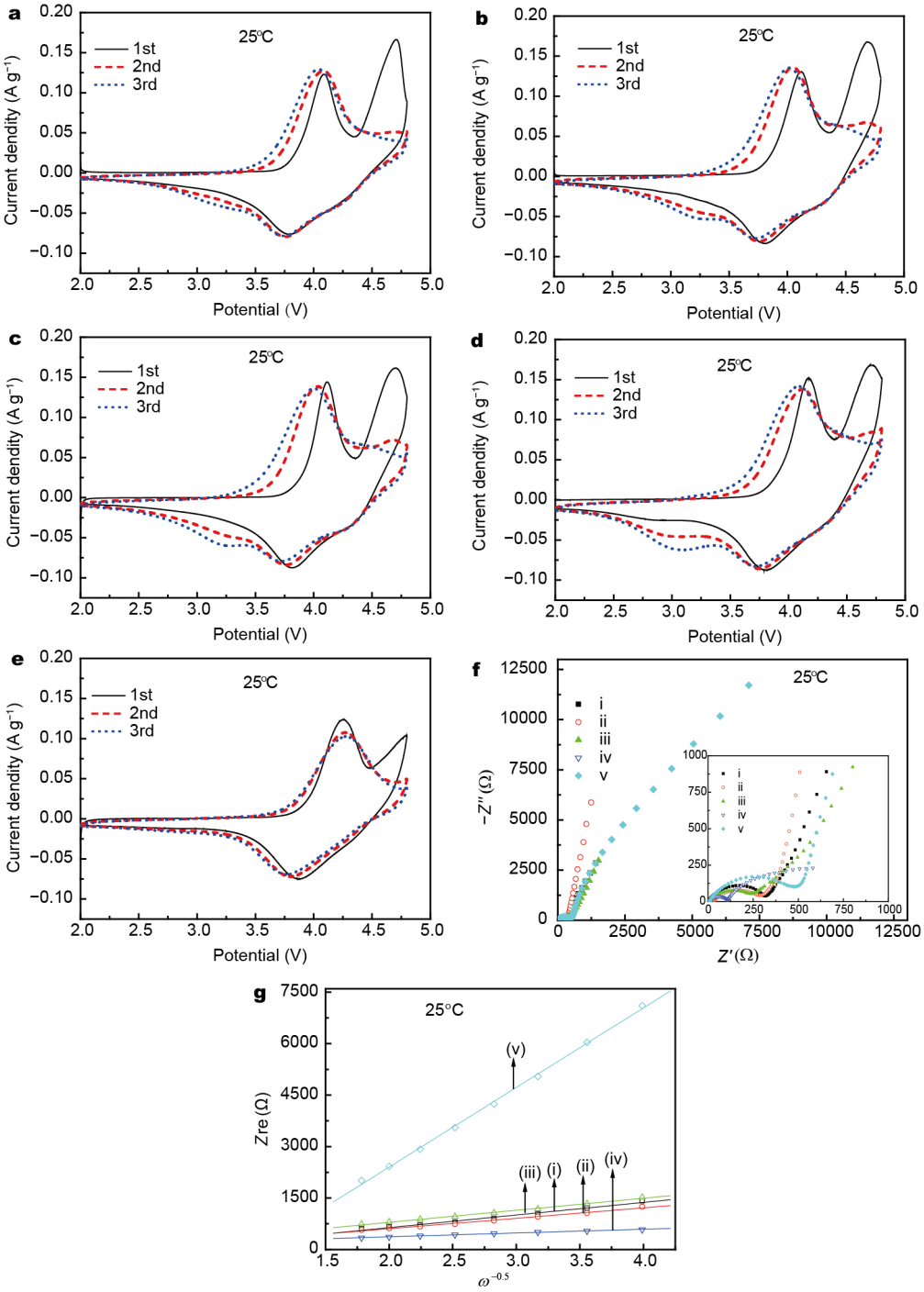


**Figure 5** CV curves of $Li_{1.2}Mn_{0.56}Ni_{0.16}Co_{0.08-x}Al_xO_2$ (a) $x$=0, (b) $x$=0.01, (c) $x$=0.02, (d) $x$=0.05, (e) $x$=0.08; (f) Nyquist plots and (g) graph of $Z_{re}$ plotted against $\omega^{-1/2}$ at low-frequency region for $Li_{1.2}Mn_{0.56}Ni_{0.16}Co_{0.08-x}Al_xO_2$ (i) $x$=0, (ii) $x$=0.01, (iii) $x$=0.02, (iv) $x$=0.05, (v) $x$=0.08.

ability of lithium-ion in the bulk of electrode material. The diffusion coefficient values by EIS can be calculated according to equation [43,44]:

$$Z_{re} = R_{ct} + R_s + \sigma\omega^{-\frac{1}{2}}, \quad (1)$$

$$D_{Li} = \frac{R^2T^2}{2A^2n^4F^4C_{Li}^2\sigma^2}, \quad (2)$$

where $A$ is the surface area of the electrode, $T$ is the absolute temperature, $R$ is the gas constant, $F$ the Faraday constant,

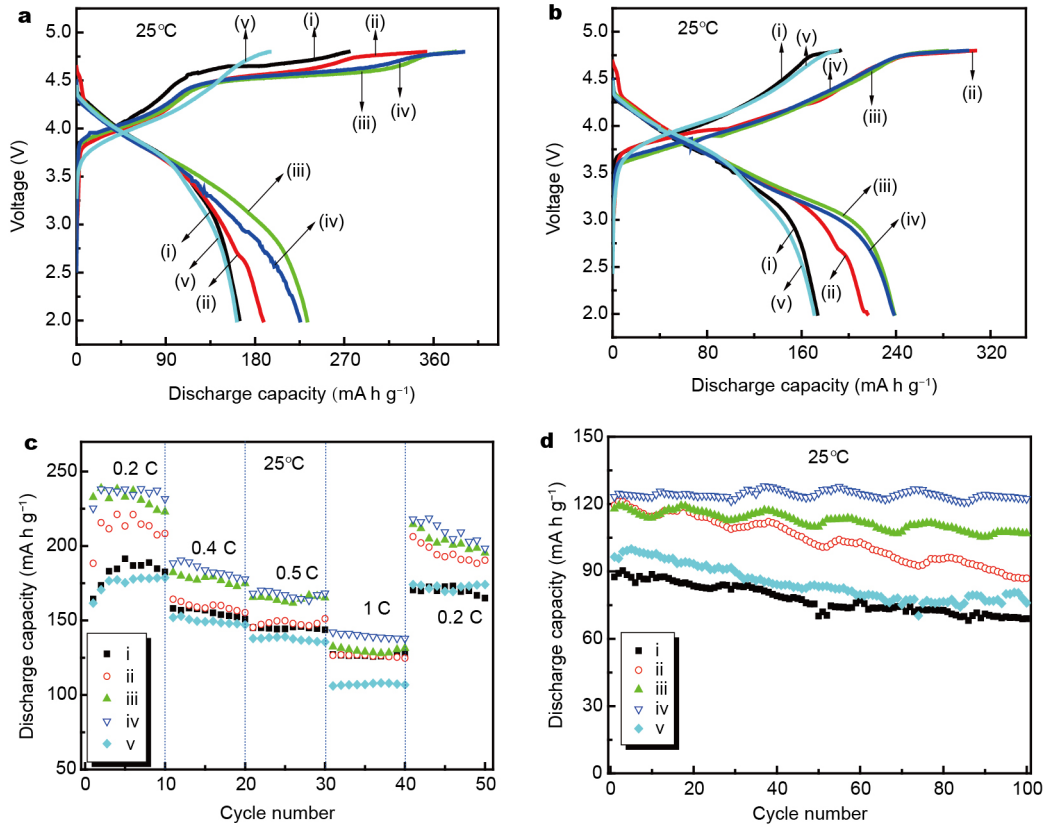


**Figure 6** (a) Initial charge/discharge profiles of $Li_{1.2}Mn_{0.56}Ni_{0.16}Co_{0.08-x}Al_xO_2$ at rate of 0.2 C, (b) the second charge-discharge curves of $Li_{1.2}Mn_{0.56}Ni_{0.16}Co_{0.08-x}Al_xO_2$ at 0.2 C, (c) rate capacity of $Li_{1.2}Mn_{0.56}Ni_{0.16}Co_{0.08-x}Al_xO_2$ at different current densities between 0.2 and 1 C and (d) cycling performance of $Li_{1.2}Mn_{0.56}Ni_{0.16}Co_{0.08-x}Al_xO_2$ at 2 C for 100 cycles (i) $x$= 0, (ii) $x$= 0.01, (iii) $x$= 0.02, (iv) $x$= 0.05, (v) $x$= 0.08.

$n$ is the number of electrons per molecule during oxidation, $C_{Li}$ is the concentration of lithium ion, $\sigma$ is the Warburg factor, which can be gained from the slope of $Z_{re}$ *vs.* $\omega^{-0.5}$ as given in Fig. 5g, and the calculated diffusion coefficients of all samples are given in Table S2. As previously reported [45,46], the diffusion overpotential is dominant when the battery discharges at high current density. Hence, the lithium-ion diffusion ability is the control step at high charge-discharge current density. It is obviously seen that Al-doping improves the diffusion coefficient of the Li-rich material, implying significantly enhanced diffusion dynamics. $Li_{1.2}Mn_{0.56}Ni_{0.16}Co_{0.08-x}Al_xO_2$ ($x$=0.05) has the highest diffusion coefficient, suggesting that it may have the highest cycling stability among all samples cycling at high current density. However, a dramatic decrease of diffusion coefficient is noted for $Li_{1.2}Mn_{0.56}Ni_{0.16}Co_{0.08-x}Al_xO_2$ ($x$=0.08) compared to the other Li-rich materials. It is postulated that high content ($x$=0.08) Al doping can block the lithium ion migration in the bulk phase of Li-rich material, and then the electronic and ionic conduction of the particles become limited.

The first and second galvanostatic charge-discharge profiles of all $Li_{1.2}Mn_{0.56}Ni_{0.16}Co_{0.08-x}Al_xO_2$ ($0 \le x \le 0.08$) samples at 0.2 C (1 C = 200 mA $g^{-1}$) rate between 2.0 and 4.8 V are presented in Figs 6a and b. A typical platform feature of layered Li-rich materials can be seen in all the charge curves. The first sloping stage below 4.4 V corresponds to the lithium extraction from layered $LiMO_2$ (M = Co, Mn, Ni) component of $Li_{1.2}Mn_{0.56}Ni_{0.16}Co_{0.08}O_2$ accompanied by the oxidation of $Co^{3+}$ to $Co^{4+}$ and $Ni^{2+}$ to $Ni^{4+}$. The voltage plateau above 4.4 V is attributed to $Li_2MnO_3$ activation based on lithium deintercalation and concomitant oxygen evolution resulting in irreversible capacity loss and low Coulombic efficiencies. In the following cycles, the Coulombic efficiencies for all samples increase due to the activation process. The initial discharge capacities of $Li_{1.2}Mn_{0.56}Ni_{0.16}Co_{0.08-x}Al_xO_2$ ($x$=0, 0.01, 0.02, 0.05 and 0.08) are 164.4, 188.3, 232.7, 225.4 and 161.7 mA h $g^{-1}$, respectively. Obviously, the Li-rich electrodes with low-level doping show a much higher initial discharge capacity than the pristine one. The differential capacity curves corresponding to the 1st and 2nd cycle are given in

Figs S2 and S3, and the voltage differences between anodic and cathodic peaks can represent the differences between charge and discharge plateau. It can be found that a small amount of Al doping can decrease the voltage differences, and then reduce the polarization of $Li_{1.2}Mn_{0.56}Ni_{0.16}Co_{0.08}O_2$ electrode during cycling.

Fig. 6c shows the rate capabilities of $Li_{1.2}Mn_{0.56}Ni_{0.16}Co_{0.08-x}Al_xO_2$ ($0 \le x \le 0.08$) samples between 0.2 and 1 C at room temperature, and the charge and discharge rates are the same. The results indicate that the Li-rich electrodes with low-level Al doping show a much higher discharge capacity than the pristine one, especially the $Li_{1.2}Mn_{0.56}Ni_{0.16}Co_{0.08-x}Al_xO_2$ ($x$=0.05) sample, which exhibits greater capacity than the other samples with charge and discharge C-rate increasing. Moreover, the capacity retention rate of the $Li_{1.2}Mn_{0.56}Ni_{0.16}Co_{0.08-x}Al_xO_2$ ($x$=0.05) is near 100% of initial value when the current was restored to 0.2 C. This result means that the $Li_{1.2}Mn_{0.56}Ni_{0.16}Co_{0.08-x}Al_xO_2$ ($x$=0.05) sample can endure great changes in current density and still retain a high cycling stability. This indicates that $Li_{1.2}Mn_{0.56}Ni_{0.16}Co_{0.08-x}Al_xO_2$ ($x$=0.05) has a strong structural stability and excellent restorability. From the above results it can be concluded that Al doping can enhance the rate-capacity and cyclic reversibility of low-Co Li-rich material. In addition, the doped Al content has a strong impact on the rate capability of $Li_{1.2}Mn_{0.56}Ni_{0.16}Co_{0.08}O_2$. The rate capacity of $Li_{1.2}Mn_{0.56}Ni_{0.16}Co_{0.08-x}Al_xO_2$ ($x$=0.08) is lower than that of the pristine one. Hence, a proper doping content of Al must be optimized to attain the best cell performance. Fast charge-discharge performance is one of the most important electrochemical properties of high-power lithium-ion batteries [47]. Fig. 6d shows the fast charge-discharge performance of all samples for 100 cycles at 2 C charge-discharge rate between 2.0 and 4.8 V at room temperature. The initial discharge capacities of $Li_{1.2}Mn_{0.56}Ni_{0.16}Co_{0.08-x}Al_xO_2$ ($x$ =0, 0.01, 0.02, 0.05 and 0.08) electrodes at 2 C are 87.5, 119.4, 117.9, 123.2 and 96.4 mA h $g^{-1}$, respectively. After 100 cycles, the discharge capacities are 68.9, 86.9, 106.9, 122.4 and 76 mA h $g^{-1}$, respectively. After 100 cycles, the corresponding capacity retention ratios are 78.7%, 72.7%, 90.6%, 99.3% and 78.8%, respectively. $Li_{1.2}Mn_{0.56}Ni_{0.16}Co_{0.08-x}Al_xO_2$ ($x$=0.05) shows the highest rate capacity and excellent cycling stability cycled at high charge-discharge rate, but the pristine one exhibits poor rate-capability. It has been reported that the lithium ion insertion/extraction kinetics corresponding to the lithium-ion diffusion in the bulk of the material affect the rate capability [48]. As mentioned above, the lithium-ion diffusion ability is the control step at high charge-discharge current density, and the charge-discharge current density significantly affects the discharge capacity. $Li_{1.2}Mn_{0.56}Ni_{0.16}Co_{0.08-x}Al_xO_2$ ($x$=0.05) has the highest lithium diffusion coefficient among all samples. The pristine one shows lower lithium diffusion coefficient and higher charge transfer resistance than Al doped one. It is therefore reasonable to infer that the increased lithium-ion mobility and reduced charge transfer resistance due to the Al doping improve the rate capability when charge-discharged at high current rates. Hence, it can be concluded that the improved rate capabilities, cycle stability, and fast charge-discharge performance of $Li_{1.2}Mn_{0.56}Ni_{0.16}Co_{0.08-x}Al_xO_2$ ($x$=0.05) can be ascribed to the improvement of lithium ion diffusion and the decrease of charge transfer resistance and electrode polarization.

The traditional $LiPF_6$-based electrolyte often suffers from oxidative decomposition at elevated temperature, and then leads to the formation of unstable solid electrolyte interface (SEI) film on the electrode surface [49,50]. Furthermore, it is easy to make thermal decomposition of $LiPF_6$ salt at elevated temperature, and then react with trace amounts of $H_2O$ accompanied by HF formation. The generating HF can result in dissolution of transition metal ions ($Mn^{2+}$, $Ni^{2+}$) [51]. The undesirable reactions significantly scarify cycling stability of the battery, especially at elevated temperature. In order to evaluate the electrochemical performance at elevated-temperature, the cycling performance was carried out at 55°C as given in Fig. 7a. The charge and discharge rate are 0.2 and 1 C, respectively. An obvious capacity difference can be noted for the two materials upon cycling. $Li_{1.2}Mn_{0.56}Ni_{0.16}Co_{0.08-x}Al_xO_2$ ($x$=0.05) exhibits higher discharge capacity than the pristine one at each cycle. However, the increasing temperature from room temperature to 55°C severely affects the cyclability, and the stability is decreased with temperature. The improved electrochemical property at elevated temperature can be understood by comparing its electrode kinetics with that at elevated-temperature. The EIS for $Li_{1.2}Mn_{0.56}Ni_{0.16}Co_{0.08-x}Al_xO_2$ ($x$=0 and 0.05) half cells after cycling at 55°C were measured at fully discharged state (about 2.0 V), and the corresponding Nyquist plots are given in Fig. 7b. The equivalent circuit used to fit the EIS is given in Fig. S4, and the $R_f$ represents the resistance of a solid electrolyte interface (SEI) film [13]. The fitted charge transfer resistances of $Li_{1.2}Mn_{0.56}Ni_{0.16}Co_{0.08-x}Al_xO_2$ ($x$=0 and 0.05) are 1616 and 769.2 Ω, respectively. Compared with $Li_{1.2}Mn_{0.56}Ni_{0.16}Co_{0.08-x}Al_xO_2$ ($x$=0 and 0.05) before cycling at room temperature, the charge transfer resistances

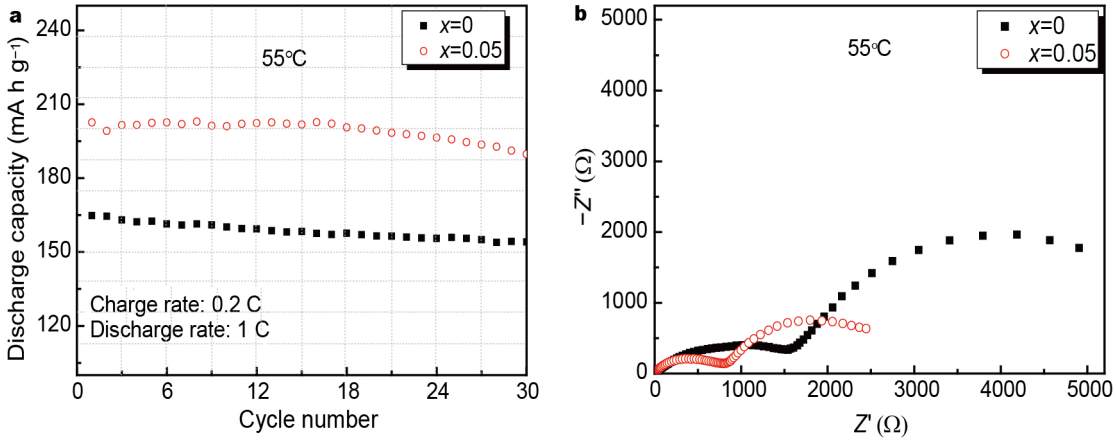


**Figure 7** (a) Cycling performance of $Li_{1.2}Mn_{0.56}Ni_{0.16}Co_{0.08-x}Al_xO_2$ ($x$=0, 0.05) at 2 C discharge rate at 55°C (charge rate is 0.2 C); (b) Nyquist plots of $Li_{1.2}Mn_{0.56}Ni_{0.16}Co_{0.08-x}Al_xO_2$ ($x$=0, 0.05) cycled at 2 C rate after cycles at 55°C.

evidently increased after cycling at elevated temperature. However, $Li_{1.2}Mn_{0.56}Ni_{0.16}Co_{0.08-x}Al_xO_2$ ($x$ = 0.05) electrode exhibits a lower charge transfer resistance than that of the pristine one. This reveals that Al doping improves the electronic conductivity of the electrode in the local environment, and increases the electrochemical activity, resulting in a relatively higher electrochemical performance at elevated temperature. On the basis of the SEI film model principle, the relation between $R_f$ and the thickness of SEI film ($l$) is as follows [52]:

$$l = \frac{R_f S}{\rho}, \tag{3}$$

where $\rho$ and $S$ is the SEI film conductivity and the surface area of the electrode, respectively. The fitted $R_f$ values of $Li_{1.2}Mn_{0.56}Ni_{0.16}Co_{0.08-x}Al_xO_2$ ($x$ = 0 and 0.05) are 2186 and 791.2 Ω, respectively. The surface area of the electrode may not change significantly during the cycling. Hence, it can be found that the film thickness of $Li_{1.2}Mn_{0.56}Ni_{0.16}Co_{0.08-x}Al_xO_2$ ($x$ = 0.05) is lower than the pristine one, indicating that Al doping contributes to the lithium ion diffusion. These features indicate that the low charge transfer resistance and thin SEI film improve lithium-ion diffusion in electrode and surface films, and then improve the discharge capacity of $Li_{1.2}Mn_{0.56}Ni_{0.16}Co_{0.08-x}Al_xO_2$ ($x$ = 0.05) at elevated temperatures. The results clearly demonstrate that the outstanding cycling stability, good rate capability, excellent fast charge-discharge performance and high capacity at elevated temperature of $Li_{1.2}Mn_{0.56}Ni_{0.16}Co_{0.08-x}Al_xO_2$ ($x$=0.05) cathode material make it a promising alternative for next generation of high-power lithium-ion batteries.

## CONCLUSION

A practical strategy was successfully developed to improve the cycling stability, rate capacity, fast charge-discharge performance and high-temperature property of low-Co $Li_{1.2}Mn_{0.56}Ni_{0.16}Co_{0.08}O_2$ cathode material by Al doping. All samples have uniform particle size of about 200–300 nm and smooth surface, and Al has been doped in the $Li_{1.2}Mn_{0.56}Ni_{0.16}Co_{0.08}O_2$ cathode material successfully and homogeneously. The suitable amount Al doping has a favorable effect on the electrochemical performance. Al doping contributes to the reversible lithium-ion insertion and extraction, and then reduces the electrochemical polarization and charge transfer resistance. The initial discharge capacities of $Li_{1.2}Mn_{0.56}Ni_{0.16}Co_{0.08-x}Al_xO_2$ ($x$ = 0, 0.01, 0.02, 0.05 and 0.08) electrodes at 2 C charge-discharge rate are 87.5, 119.4, 117.9, 123.2 and 96.4 mA h $g^{-1}$, respectively. After 100 cycles, the discharge capacities are 68.9, 86.9, 106.9, 122.4 and 76 mA h $g^{-1}$, respectively. After 100 cycles, the corresponding capacity retention ratios are 78.7%, 72.7%, 90.6%, 99.3% and 78.8%, respectively. $Li_{1.2}Mn_{0.56}Ni_{0.16}Co_{0.08-x}Al_xO_2$ ($x$=0.05) also exhibits high discharge capacity than the pristine one at each cycle at 55°C. The improved electrode performance of $Li_{1.2}Mn_{0.56}Ni_{0.16}Co_{0.08-x}Al_xO_2$ ($x$ = 0.05) is clearly related to the improved reversibility of lithium-ion insertion and extraction, enhanced lithium-ion diffusion coefficient, decreased charge transfer resistance, and reduced electrochemical polarization. Therefore, outstanding cycling stability, good rate capability, excellent fast charge-discharge performance and high capacity at elevated temperature of $Li_{1.2}Mn_{0.56}Ni_{0.16}Co_{0.08-x}Al_xO_2$ ($x$=0.05) cathode material make it a competitive candidate for next generation of high-power lithium-ion batteries.

**Received 8 July 2016; accepted 26 July 2016; published online 18 August 2016**


1 Li W, Zeng L, Wu Y, *et al.* Nanostructured electrode materials for lithium-ion and sodium-ion batteries via electrospinning. Sci China Mater, 2016, 59: 287–321
2 Zhang J, Yu A. Nanostructured transition metal oxides as advanced anodes for lithium-ion batteries. Sci Bull, 2015, 60: 823–838
3 Song L, Yang S, Wei W, *et al.* Hierarchical $SnO_2$ nanoflowers assembled by atomic thickness nanosheets as anode material for lithium ion battery. Sci Bull, 2015, 60: 892–895
4 Wang L, Hu Z, Zhao K, *et al.* Hollow spherical $LiNi_{0.5}Mn_{1.5}O_4$ built from polyhedra with high-rate performance via carbon nanotube modification. Sci China Mater, 2016, 59: 95–103
5 Wu C, Yuan L, Li Z, *et al.* High-performance lithium-selenium battery with Se/microporous carbon composite cathode and carbonate-based electrolyte. Sci China Mater, 2015, 58: 91–97
6 Sun X, Yan C, Chen Y, *et al.* Three-dimensionally "curved" NiO nanomembranes as ultrahigh rate capability anodes for Li-ion batteries with long cycle lifetimes. Adv Energy Mater, 2014, 4: 1300912
7 Massé RC, Uchaker E, Cao G. Beyond Li-ion: electrode materials for sodium- and magnesium-ion batteries. Sci China Mater, 2015, 58: 715–766
8 Liu X, Su Q, Zhang C, *et al.* Enhanced electrochemical performance of $Li_{1.2}Mn_{0.54}Ni_{0.13}Co_{0.13}O_2$ cathode with an ionic conductive $LiVO_3$ coating layer. ACS Sustain Chem Eng, 2016, 4: 255–263
9 Sun YY, Li F, Qiao QQ, *et al.* Surface modification of $Li(Li_{0.17}Ni_{0.2}Co_{0.05}Mn_{0.58})O_2$ with $LiAlSiO_4$ fast ion conductor as cathode material for Li-ion batteries. Electrochim Acta, 2015, 176: 1464–1475
10 Nayak PK, Grinblat J, Levi E, *et al.* Effect of cycling conditions on the electrochemical performance of high capacity Li and Mn-rich cathodes for Li-ion batteries. J Power Sources, 2016, 318: 9–17
11 Zhuo H, Zhang Y, Wang D, *et al.* Insight into lithium-rich layered cathode materials $Li[Li_{0.1}Ni_{0.45}Mn_{0.45}]O_2$ *in situ* coated with graphene-like carbon. Electrochim Acta, 2014, 149: 42–48
12 Zhao E, Liu X, Hu Z, *et al.* Facile synthesis and enhanced electrochemical performances of $Li_2TiO_3$-coated lithium-rich layered $Li_{1.13}Ni_{0.30}Mn_{0.57}O_2$ cathode materials for lithium-ion batteries. J Power Sources, 2015, 294: 141–149
13 Xiang Y, Li J, Wu X, *et al.* Synthesis and electrochemical characterization of Mg-doped Li-rich Mn-based cathode material. Ceramics Int, 2016, 42: 8833–8838
14 Li L, Song BH, Chang YL, *et al.* Retarded phase transition by fluorine doping in Li-rich layered $Li_{1.2}Mn_{0.54}Ni_{0.13}Co_{0.13}O_2$ cathode material. J Power Sources, 2015, 283: 162–170
15 Zhao Y, Xia M, Hu X, *et al.* Effects of Sn doping on the structural and electrochemical properties of $Li_{1.2}Ni_{0.2}Mn_{0.8}O_2$ Li-rich cathode materials. Electrochim Acta, 2015, 174: 1167–1174
16 Huang Z, Wang Z, Jing Q, *et al.* Investigation on the effect of Na doping on structure and Li-ion kinetics of layered $LiNi_{0.6}Co_{0.2}Mn_{0.2}O_2$ cathode material. Electrochim Acta, 2016, 192: 120–126
17 Oh P, Myeong S, Cho W, *et al.* Superior long-term energy retention and volumetric energy density for Li-rich cathode materials. Nano Lett, 2014, 14: 5965–5972
18 Lee Y, Kim MG, Cho J. Layered $Li_{0.88}[Li_{0.18}Co_{0.33}Mn_{0.49}]O_2$ nanowires for fast and high capacity Li-Ion storage material. Nano Lett, 2008, 8: 957–961
19 Yan J, Liu X, Li B. Recent progress in Li-rich layered oxides as cathode materials for Li-ion batteries. RSC Adv, 2014, 4: 63268–63284
20 Toprakci O, Toprakci HAK, Li Y, *et al.* Synthesis and characterization of $xLi_2MnO_3{\cdot}(1-x)LiMn_{1/3}Ni_{1/3}Co_{1/3}O_2$ composite cathode materials for rechargeable lithium-ion batteries. J Power Sources, 2013, 241: 522–528
21 Yi TF, Tao W, Chen B, *et al.* High-performance $xLi_2MnO_3{\cdot}(1-x)LiMn_{1/3}Co_{1/3}Ni_{1/3}O_2$ $(0.1\leq x\leq 0.5)$ as cathode material for lithium-ion battery. Electrochim Acta, 2016, 188: 686–695
22 Ghanty C, Basu RN, Majumder SB. Electrochemical characteristics of $xLi_2MnO_2$-$(1-x)Li(Mn_{0.375}Ni_{0.375}Co_{0.25})O_2$ $(0.0\leq x\leq 1.0)$ composite cathodes: effect of particle and $Li_2MnO_2$ domain size. Electrochim Acta, 2014, 132: 472–482
23 Zhang Q, Peng T, Zhan D, *et al.* Synthesis and electrochemical property of $xLi_2MnO_2{\cdot}(1-x)LiMnO_2$ composite cathode materials derived from partially reduced $Li_2MnO_3$. J Power Sources, 2014, 250: 40–49
24 He P, Yu H, Li D, *et al.* Layered lithium transition metal oxide cathodes towards high energy lithium-ion batteries. J Mater Chem, 2012, 22: 3680
25 Ye D, Wang B, Chen Y, *et al.* Understanding the stepwise capacity increase of high energy low-Co Li-rich cathode materials for lithium ion batteries. J Mater Chem A, 2014, 2: 18767–18774
26 Huang X, Wang M, Che R. Modulating the $Li^+/Ni^{2+}$ replacement and electrochemical performance optimizing of layered lithium-rich $Li_{1.2}Ni_{0.2}Mn_{0.6}O_2$ by minor Co dopant. J Mater Chem A, 2014, 2: 9656–9665
27 Fan J, Li G, Luo D, *et al.* Hydrothermal-assisted synthesis of Li-rich layered oxide microspheres with high capacity and superior rate-capability as a cathode for lithium-ion batteries. Electrochim Acta, 2015, 173: 7–16
28 Yi TF, Mei J, Zhu YR. Key strategies for enhancing the cycling stability and rate capacity of $LiNi_{0.5}Mn_{1.5}O_4$ as high-voltage cathode materials for high power lithium-ion batteries. J Power Sources, 2016, 316: 85–105
29 Yi T, Hu X, Gao K. Synthesis and physicochemical properties of $LiAl_{0.05}Mn_{1.95}O_4$ cathode material by the ultrasonic-assisted sol-gel method. J Power Sources, 2006, 162: 636–643
30 Liu L, Xie F, Lyu J, *et al.* Tin-based anode materials with well-designed architectures for next-generation lithium-ion batteries. J Power Sources, 2016, 321: 11–35
31 Zhao R, Zhang S, Liu J, *et al.* A review of thermal performance improving methods of lithium ion battery: electrode modification and thermal management system. J Power Sources, 2015, 299: 557–577
32 Yang C, Zhang Q, Ding W, *et al.* Improving the electrochemical performance of layered lithium-rich cathode materials by fabricating a spinel outer layer with $Ni^{3+}$. J Mater Chem A, 2015, 3: 7554–7559
33 Thackeray MM, Kang SH, Johnson CS, *et al.* $Li_2MnO_3$-stabilized $LiMO_2$ (M = Mn, Ni, Co) electrodes for lithium-ion batteries. J Mater Chem, 2007, 17: 3112–3125
34 Chen Z, Dahn JR. Effect of a $ZrO_2$ coating on the structure and electrochemistry of $Li_xCoO_2$ when cycled to 4.5 V. Electrochem Solid-State Lett, 2002, 5: A213
35 Wang CC, Lin YC, Chou PH. Mitigation of layer to spinel conversion of a lithium-rich layered oxide cathode by substitution of Al in a lithium ion battery. RSC Adv, 2015, 5: 68919–68928
36 Shannon RD. Revised effective ionic radii and systematic studies of interatomic distances in halides and chalcogenides. Acta Cryst A, 1976, 32: 751–767
37 Mohanty D, Sefat AS, Kalnaus S, *et al.* Investigating phase transformation in the $Li_{1.2}Co_{0.1}Mn_{0.55}Ni_{0.15}O_2$ lithium-ion battery cath-

ode during high-voltage hold (4.5 V) via magnetic, X-ray diffraction and electron microscopy studies. J Mater Chem A, 2013, 1: 6249–6261
38 Zheng Z, Wu ZG, Zhong YJ, *et al.* A further electrochemical investigation on solutions to high energetical power sources: isomerous compound $0.75Li_{1.2}Ni_{0.2}Mn_{0.6}O_2{\cdot}0.25LiNi_{0.5}Mn_{1.5}O_4$. RSC Adv, 2015, 5: 37330–37339
39 Wang D, Zhao Y, Xu X, *et al.* Novel $Li_2MnO_3$ nanowire anode with internal Li-enrichment for use in a Li-ion battery. Nanoscale, 2014, 6: 8124–8129
40 Zhang X, Yin Y, Hu Y, *et al.* Zr-containing phosphate coating to enhance the electrochemical performances of Li-rich layer-structured $Li[Li_{0.2}Ni_{0.17}Co_{0.07}Mn_{0.56}]O_2$. Electrochim Acta, 2016, 193: 96–103
41 Pang S, Wang Y, Chen T, *et al.* The effect of $AlF_3$ modification on the physicochemical and electrochemical properties of Li-rich layered oxide. Ceramics Int, 2016, 42: 5397–5402
42 Yu FD, Wang ZB, Chen F, *et al.* Crystal structure and multicomponent effects in $Li_{1+x}Mn_{2-x-y}Al_yO_4$ cathode materials for Li-ion batteries. J Power Sources, 2014, 262: 104–111
43 Liu H, Wen G, Bi S, *et al.* High rate cycling performance of nanosized $Li_4Ti_5O_{12}$/graphene composites for lithium ion batteries. Electrochim Acta, 2016, 192: 38–44
44 Xiang X, Li W. Self-directed chemical synthesis of lithium-rich layered oxide $Li[Li_{0.2}Ni_{0.2}Mn_{0.6}]O_2$ with tightly interconnected particles as cathode of lithium ion batteries with improved rate capability. Electrochim Acta, 2014, 127: 259–265
45 Wu MS, Chiang PCJ, Lin JC. Electrochemical investigations on advanced lithium-ion batteries by three-electrode measurements. J Electrochem Soc, 2005, 152: A47–A52
46 Yi TF, Fang ZK, Xie Y, *et al.* Synthesis of $LiNi_{0.5}Mn_{1.5}O_4$ cathode with excellent fast charge-discharge performance for lithium-ion battery. Electrochim Acta, 2014, 147: 250–256
47 Sun X, Si W, Liu X, *et al.* Multifunctional Ni/NiO hybrid nanomembranes as anode materials for high-rate Li-ion batteries. Nano Energy, 2014, 9: 168–175
48 Liu J, Manthiram A. Understanding the improved electrochemical performances of Fe-substituted 5 V spinel cathode $LiMn_{1.5}Ni_{0.5}O_4$. J Phys Chem C, 2009, 113: 15073–15079
49 Duncan H, Duguay D, Abu-Lebdeh Y, *et al.* Study of the $LiMn_{1.5}Ni_{0.5}O_4$/electrolyte interface at room temperature and 60°C. J Electrochem Soc, 2011, 158: A537
50 Lu D, Xu M, Zhou L, *et al.* Failure mechanism of graphite/$LiNi_{0.5}Mn_{1.5}O_4$ cells at high voltage and elevated temperature. J Electrochemical Soc, 2013, 160: A3138–A3143
51 Chen J, Zhang H, Wang M, *et al.* Improving the electrochemical performance of high voltage spinel cathode at elevated temperature by a novel electrolyte additive. J Power Sources, 2016, 303: 41–48
52 Jafta CJ, Ozoemena KI, Mathe MK, *et al.* Synthesis, characterisation and electrochemical intercalation kinetics of nanostructured aluminium-doped $Li[Li_{0.2}Mn_{0.54}Ni_{0.13}Co_{0.13}]O_2$ cathode material for lithium ion battery. Electrochim Acta, 2012, 85: 411–422

**Acknowledgments** This work was supported by Anhui Provincial Natural Science Foundation (1508085MB25), the National Natural Science Foundation of China (51274002 and 51404002), Anhui Provincial Science Fund for Excellent Young Scholars (gxyqZD2016066), and the Program for Innovative Research Team in Anhui University of Technology (TD201202).

**Author contributions** Yi TF conceived the strategy, supervised the design of experiments, and wrote the manuscript, and all authors participated in the review of the manuscript. Han X, Yang SY performed the materials synthesis, characterization and electrochemical measurements. Zhu YR was involved in data analysis and discussion.

**Conflict of interest** The authors declare that they have no conflict of interest.

**Supplementary information** Supplementary data are available in the online version of the paper.

**Ting-Feng Yi** received his BE degree in chemical engineering and technology from Liaocheng University in 2001. He then obtained MSc degree in applied chemistry in 2004 and PhD degree in chemical engineering and technology from Harbin Institute of Technology in 2007. He joined Anhui University of Technology as an assistant professor of chemistry in 2007. He is currently the professor of Anhui University of Technology, China. His research interests include synthesis of electrochemical functional materials and their application in lithium-ion battery and lead-acid battery. For detail please see his researcher ID: http://www.researcherid.com/rid/F-4594-2012.

## 提高富锂低钴的$Li_{1.2}Mn_{0.56}Ni_{0.16}Co_{0.08-x}Al_xO_2$ ($0\leqslant x\leqslant 0.08$)正极材料的电化学性能

伊廷锋*, 韩啸, 杨双瑗, 朱彦荣

**摘要** 本文采用溶胶凝胶法成功合成了层状$Li_{1.2}Mn_{0.56}Ni_{0.16}Co_{0.08-x}Al_xO_2$ ($0\leqslant x\leqslant 0.08$)正极材料. XRD及其精细结果表明, 所有的材料均具有典型的α-$NaFeO_2$结构, 属于*R*-3*m*空间群. Al掺杂后的材料晶胞参数*a*值几乎不变, 但是*c*值和晶胞体积略微减小. SEM和HRTEM证明了所有样品均具有200 – 300 nm的均一粒径和光滑的表面. EDS谱图说明Al已经成功地进入了$Li_{1.2}Mn_{0.56}Ni_{0.16}Co_{0.08}O_2$正极材料的晶格. CV和EIS说明适量的Al掺杂有利于锂离子的可逆脱嵌, 减小了材料的电化学极化和电荷转移电阻. 在所有样品中, $Li_{1.2}Mn_{0.56}Ni_{0.16}Co_{0.08-x}Al_xO_2$ ($x$=0.05)展示了最小的电荷转移电阻和最高的锂离子扩散系数. 电化学性能测试表明, 少量Al掺杂的富锂电极具有比纯样更高的放电容量, 特别是$Li_{1.2}Mn_{0.56}Ni_{0.16}Co_{0.08-x}Al_xO_2$ ($x$=0.05)样品具有比其他样品更高的倍率容量和更好的快速充放电性能. 55°C时, $Li_{1.2}Mn_{0.56}Ni_{0.16}Co_{0.08-x}Al_xO_2$ ($x$=0.05)展示了比纯样更高的放电容量. 高的倍率容量、好的高倍率循环稳定性以及优秀的高温性能使得低钴$Li_{1.2}Mn_{0.56}Ni_{0.16}Co_{0.08-x}Al_xO_2$ ($x$=0.05)材料成为下一代锂离子电池颇具前景的选择.